J|A|C|S
ARTICLES
Published on Web 09/26/2003

Size- and Support-Dependent Electronic and Catalytic Properties of Au^0/Au^{3+} Nanoparticles Synthesized from Block Copolymer Micelles

B. Roldan Cuenya, Sung-Hyeon Baeck, Thomas F. Jaramillo, and Eric W. McFarland*

Contribution from the Department of Chemical Engineering, University of California-Santa Barbara, Santa Barbara, California 93106

Received June 2, 2003; E-mail: mcfar@engineering.ucsb.edu

Abstract: Supported Au nanoclusters synthesized from diblock copolymer micelles can be reliably prepared with well-controlled sizes and dispersions. For particles with diameters between approximately 1 and 6 nm, the particle size and the support were found to strongly influence the oxygen reactivity, the formation and stabilization of a metal-oxide, and the catalytic activity for electrooxidation of carbon monoxide. The smallest particles studied (1.5 nm) were the most active for electrooxidation of CO and had the largest fraction of oxygen associated with gold at the surface as measured by the Au^{3+}/Au^0 X-ray photoemission intensities. Conducting and semiconducting substrates, ITO-coated glass and TiO_2, respectively, were associated with greater stabilization of Au^{3+} oxide as compared to insulating, SiO_2, substrates.

Introduction

Although gold is relatively inert in its bulk form, particles with dimensions less than 10 nm have interesting and unexpected electronic and catalytic properties.[1−4] Haruta first reported the high catalytic activity of Au nanoparticles supported on metal oxides for low-temperature CO oxidation[5] and for the selective epoxidation of propene.[5,6]

In the past decade, highly dispersed gold catalysts have been shown to be active (and very selective) for many other reactions important in industry such as low-temperature water gas shift reactions and NO reduction with hydrocarbons.[1,4,6−16] Previously, attention has been given to the size dependency on activity and selectivity and to the importance of the cluster−support interactions.[1,11,15−20] In general, it has been found that incompletely coordinated surface atoms on small metal nanoparticles, and defects on the metal oxide support, constitute the most reactive sites. Häkkinen et al.[20] have recently shown that the activity of Au nanoclusters can also be affected by charge transfer from the oxide support to the nanoparticle. Using size-selected small Au nanoclusters supported on MgO(100), they found that surface oxygen vacancies play a dominant role not just in anchoring the metal clusters, but also in activating the clusters by partial charge transfer.

Several specific reaction pathways are under discussion; however, most researchers agree with the necessity of selecting an appropriate nanocluster−oxide support combination that allows dissociation of reactants and stabilization of intermediate products to obtain the enhanced activities and selectivities as compared to bulk homogeneous materials.

The recent report by Boyen et al.[21] of the nonmonotonic size-dependent oxide stability of gold nanoparticles supported on SiO_2 is of great interest and may relate directly to catalytic properties in the presence of oxygen. This important work, however, left several relevant questions open. The Au particle sizes found to be resistant to oxidation were grown by chemical stabilization of closed-shell clusters with a $(PPh_3)_{12}Cl_6$ ligand, whereas the sizes that were not resistant to oxidation were formed in diblock copolymer micelles. Thus, the question arises as to the role of the preparation route. Given the small difference in size between the oxidation resistant and nonresistant clusters, ±0.2 nm (determined by AFM), the chemical reactivity differ-

(1) Haruta, M. *Cattech* **2002**, *6*, 102−115.
(2) Mason, M. G.; Lee, S. T.; Apai, G. *Chem. Phys. Lett.* **1980**, *76*, 51−53.
(3) Wertheim, G. K.; DiCenzo, S. B.; Youngquist, S. E. *Phys. Rev. Lett.* **1983**, *51*, 2310−2313.
(4) Valden, M.; Lai, X.; Goodman, D. W. *Science* **1998**, *281*, 1647−1650.
(5) Haruta, M.; Yamada, N.; Kobayashi, T.; Iijima, S. *J. Catal.* **1989**, *115*, 301.
(6) Haruta, M.; Uphade, B. S.; Tsubota, S.; Miyamoto, A. *Res. Chem. Intermed.* **1998**, *24*, 329−336.
(7) Bamwenda, G. R.; Tsubota, S.; Nakamura, T.; Haruta, M. *Catal. Lett.* **1997**, *44*, 83−87.
(8) Boccuzzi, F.; Chiorino, A.; Tsubota, S.; Haruta, M. *J. Phys. Chem.* **1996**, *100*, 3625−3631.
(9) Haruta, M.; Tsubota, S.; Kobayashi, T.; Kageyama, H.; Genet, M. J.; Delmon, B. *J. Catal.* **1993**, *144*, 175−192.
(10) Haruta, M.; Ueda, A.; Tsubota, S.; Sanchez, R. M. T. *Catal. Today* **1996**, *29*, 443−447.
(11) Haruta, M. *Catal. Today* **1997**, *36*, 153−166.
(12) Haruta, M.; Date, M. *Appl. Catal., A* **2001**, *222*, 427−437.
(13) Iizuka, Y.; Fujiki, H.; Yamauchi, N.; Chijiiwa, T.; Arai, S.; Tsubota, S.; Haruta, M. *Catal. Today* **1997**, *36*, 115−123.
(14) Tsubota, S.; Nakamura, T.; Tanaka, K.; Haruta, M. *Catal. Lett.* **1998**, *56*, 131−135.
(15) Valden, M.; Pak, S.; Lai, X.; Goodman, D. W. *Catal. Lett.* **1998**, *56*, 7−10.
(16) Valden, M.; Goodman, D. W. *Isr. J. Chem.* **1998**, *38*, 285−292.
(17) Rodriguez, J. A.; Liu, G.; Jirsak, T.; Hrbek, J.; Chang, Z. P.; Dvorak, J.; Maiti, A. *J. Am. Chem. Soc.* **2002**, *124*, 5242−5250.
(18) Vijay, A.; Mills, G.; Metiu, H. *J. Chem. Phys.* **2003**, *118*, 6536−6551.
(19) Molina, L. M.; Hammer, B. *Phys. Rev. Lett.* **2003**, *90*, 206102.
(20) Häkkinen, H.; Abbet, W.; Sanchez, A.; Heiz, U.; Landman, U. *Angew. Chem., Int. Ed.* **2003**, *42*, 1297−1300.
(21) Boyen, H. G.; Kastle, G.; Weigl, F.; Koslowski, B.; Dietrich, C.; Ziemann, P.; Spatz, J. P.; Riethmuller, S.; Hartmann, C.; Moller, M.; Schmid, G.; Garnier, M. G.; Oelhafen, P. *Science* **2002**, *297*, 1533−1536.

10.1021/ja036468u CCC: $25.00

ences attributed by the authors to size (and shell closure of Au_{55}) could also be a result of the different chemistries (and residues) of the preparation routes.

To further investigate the important observation of size-dependent reactivity, we have extended the preliminary work of Boyen et al. and used an identical preparation procedure for all clusters studied. This method is known as micelle encapsulation. The cluster size is varied by changing only the length of the block copolymer head. In this work, we addressed the following questions using gold nanoclusters prepared by identical synthetic routes: (1) What are the size-dependent electronic properties of supported Au nanoclusters? (2) What properties are altered by changing the supports? (3) Is there a correlation between catalytic activity for CO oxidation and any size-dependent propensity for oxidation? (4) Can Au-oxide be stabilized on the nanocluster surface? (5) How does the presence of Au-oxide affect the activity of the nanocluster as catalysts?

Experimental Section

Commercial (Polymer Source, Inc.) block copolymers of poly(styrene)-*block*-poly(2-vinylpyridine) (PS-*b*-P2VP) of different molecular weight and PS_{mw}/PVP_{mw} ratios were used to encapsulate Au nanoparticles (0.5−10 nm). Following Spatz et al.,[22] a 0.5 wt % solution ($c = 5$ mg/mL) of the diblock copolymer PS(x)-*b*-P2VP(y) (54 300/8800 g/mol, 81 000/14 200 g/mol, and 53 000/43 800 g/mol) was prepared in toluene ($V = 5$ mL) and stirred for 4 h. Later, a fixed ratio of the metal precursor ($HAuCl_4 \cdot 3H_2O$, 7.4 mg) per pyridine unit (0.6/1 ratio) was added to the solution under nitrogen in a glovebox and stirred for 48 h. The $AuCl_4^-$ ions were bound as counterions to the pyridine units of the polar core of the micelles. A relative gold/2VP ratio of 0.6/1 was held constant throughout, and different cluster sizes were obtained by changing the size of the polymer head. For additional preparation details, see refs 22−24.

As substrates, we used the following: (1) natively oxidized, n-doped Si(001) wafers; (2) natively oxidized Ti(15 nm) (electron beam evaporated under high vacuum conditions) on n-Si(001); (3) natively oxidized polycrystalline Ti-foil (99.5% purity); and (4) 200 nm ITO films (In_2O_3 (90%)−SnO_2 (10%)) coated on glass (Delta Technologies, Inc.). The substrates were dip-coated with a monolayer of micelles at 6 mm/min. The dip-coated substrates were dried by exposure to N_2. After being dip-coated, the polymer was removed using an oxygen plasma (110 W, 300 mTorr, 10 min) treatment. Such a treatment also causes the reduction of Au^{3+} to Au^0 (by oxidation of the micellar components) and allows the gold in the micelle to nucleate to a nanometer-sized crystalline Au particle.[21,22,25] Complete removal of the polymer was assured by an X-ray photoelectron spectroscopy (XPS) carbon signal.

All samples were transferred to the XPS chamber immediately after atomic oxygen exposure and were pumped to high vacuum conditions (10^{-8} Torr) within 1 h to minimize uncertainties in the relative Au^{3+} content due to a possible decomposition to Au^0.[26]

The size, order, and dispersion of the Au nanoparticles produced by the micellar block copolymer synthesis method were characterized before and after oxygen plasma treatment by atomic force microscopy (AFM, Digital Instruments D-3000) operating in tapping mode (non-contact), and by a transmission electron microscope (TEM, JEOL 2000 FX).

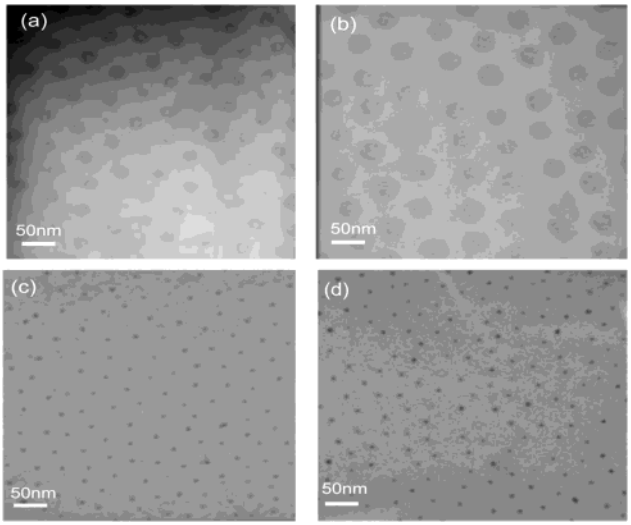

Figure 1. TEM photographs of Au nanoclusters synthesized using polymers with two different head sizes: PS(81000)-P2VP(14200) (a−c) and PS-(53000)-P2VP(43800) (b−d) supported on TiO_2/Ti(50 nm)/Cu-grid. Images a and b were taken before O_2-plasma treatment, and (c) and (d) were taken after treatment.

The binding energies of the conduction and valence band electrons of the oxide-supported smaller Au clusters were measured by XPS (Kratos, Axis Ultra). Monochromatic Al K_α radiation was used for excitation (1486.6 eV), and the photoelectrons were detected with a multichannel detector with 8 channeltrons. The measured spectra were fit by least-squares to a product of Gaussian−Lorentzian functions after subtraction of shirley background noise. Raw data were deconvoluted to four subspectra with binding energies corresponding to Au^0 (84.0 and 87.7 eV, solid vertical lines) and Au_2O_3 (85.8 and 89.5 eV,[21,27] dotted vertical lines).

The raw data were corrected for substrate charging using the binding energy of the O-1s peak on TiO_2 (530.0 eV) for the Au/TiO_2/Ti(15 nm)/Si(001) and Au/TiO_2/Ti-foil samples, and using the Si-2p peak (103.3 eV) on SiO_2 for the Au/SiO_2/Si(001) system as references.

Electrocatalytic CO oxidation measurements of Au nanoparticles coated on ITO were performed (after polymer removal by oxygen plasma) in 30 mL of 0.5 M KOH solution (ACS grade). A gas sealed electrochemical cell was used to conduct the CO electrooxidation experiments. The cell housed three electrodes (sample working electrode, Pt mesh counter electrode, and Ag/AgCl reference electrode). The inlet reactant gas passed through an immersed tube capped by a gas-diffusion frit to facilitate gas−liquid saturation. The 0.5 M KOH solution was saturated with 99.998% N_2 for 15 min with light stirring prior to the first cyclic voltammogram. To "activate" the Au nanoparticles for electrocatalysis, 30 cyclic voltammograms were then measured from −0.2 to +0.7 V versus the Ag/AgCl reference electrode, at a scan rate of 0.3 V/s. [25] The electrolyte was subsequently saturated with 99.5% CO for 20 min. Sixty cyclic voltammograms were then measured for CO electrooxidation, from −0.4 to +0.8 V versus the reference electrode at a rate of 0.3 V/s.

Results

Cluster Size: AFM/TEM. Figures 1 and 2 show micrographs obtained by TEM and AFM of Au clusters synthesized using polymers with two different head sizes: PS(81000)-P2VP-(14200) (a−c), and PS(53000)-P2VP(43800) (b−d). The top images (Figures 1, 2a,b) were taken before polymer removal,

(22) Spatz, J. P.; Mossmer, S.; Hartmann, C.; Moller, M.; Herzog, T.; Krieger, M.; Boyen, H. G.; Ziemann, P.; Kabius, B. *Langmuir* **2000**, *16*, 407−415.
(23) Haupt, M.; Miller, S.; Ladenburger, A.; Sauer, R.; Thonke, K.; Spatz, J. P.; Riethmuller, S.; Moller, M.; Banhart, F. *J. Appl. Phys.* **2002**, *91*, 6057−6059.
(24) Tamil Selvan, S.; Hayakawa, T.; Nogami, M.; Moller, M. *J. Phys. Chem. B* **1999**, *103*, 7441−7448.
(25) Jaramillo, T. F.; Baeck, S. H.; Roldan Cuenya, B.; McFarland, E. W. *J. Am. Chem. Soc.* **2003**, *125*, 7148.
(26) Tsai, H. C.; Hu, E.; Perng, K.; Chen, M. K.; Wu, J. C.; Chang, Y. S. *Surf. Sci. Lett.* **2003**, *537*, L447.
(27) Koslowski, B.; Boyen, H. G.; Wilderotter, C.; Kastle, G.; Ziemann, P.; Wahrenberg, R.; Oelhafen, P. *Surf. Sci.* **2001**, *475*, 1−10.

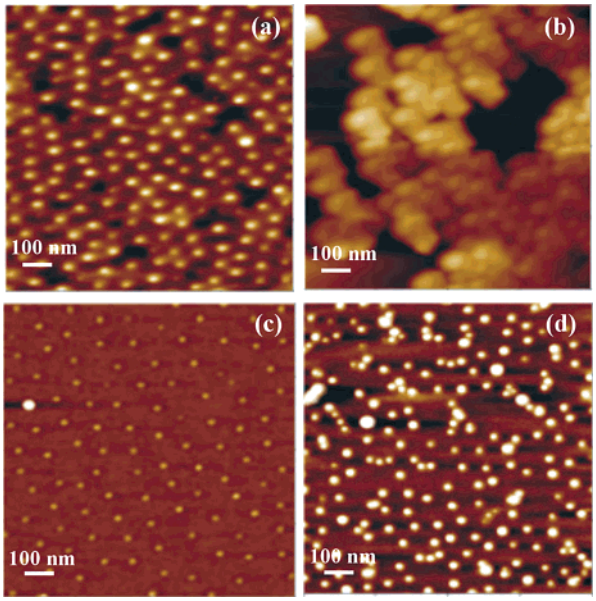

Figure 2. AFM images of Au nanoparticles synthesized using polymers with two different head sizes: PS(81000)-P2VP(14200) (a−c) and PS-(53000)-P2VP(43800) (b−d) supported on SiO_2/Si(001). Images (a) and (b) were taken before polymer etch under O_2-plasma treatment, and (c) and (d) were taken after treatment. The height scales are (a) $z = 20$ nm, (b) $z = 40$ nm, (c) $z = 15$ nm, (d) $z = 5$ nm.

and the bottom images (Figures 1, 2c,d) were taken after removal of the polymer (by oxygen plasma). The AFM images correspond to Au nanoparticles dip-coated on natively oxidized Si(001) wafers, and the TEM images correspond to Au particles drop-casted on a Ti-coated (50 Å) microscopy grid.

The TEM images in Figure 1a and b (taken before polymer removal and Au^{3+} reduction) show a fine grain substructure (i.e., regions with higher electron densities) inside every micelle corresponding to gold particles (from tetrachloroauric acid) selectively attached to the pyridine units within the P2VP micelle core. Figure 1c and d shows the decrease in cluster size caused by the plasma treatment together with the reduction of Au^{3+} to Au^0.

Figure 1a,b shows that the Au-micelles preferentially arrange to form a quasi hexagonal pattern. After the organics were removed from the micelles, the hexagonal pattern remains (Figure 1c,d). The sizes of the polymer-encapsulated Au particles before O_2-plasma were estimated by AFM to be 30 ± 5 nm (Figure 2b), 15 ± 5 nm (Figure 2a), and 10 ± 5 nm (not shown) on SiO_2/Si(001), in reasonable agreement with the TEM data that showed micelle core sizes of 25 ± 1.5 nm (Figure 1b), 13 ± 1 nm (Figure 1a), and 10 ± 1.5 nm (not shown).

From TEM images of Au nanoparticles after oxygen treatment (Figure 1c,d), Gaussian size distributions with average cluster diameters of 6.0 ± 1.5, 4.0 ± 1.0, and 1.5 ± 1.3 nm were observed for the three polymers. AFM image analysis reported slightly larger values (7.0 ± 1.3, 5.0 ± 1.0, 1.5 ± 1.1 nm, respectively). The particle height has been used as a size-representative parameter for AFM instead of its diameter because it minimizes the tip broadening effect. The cluster heights determined are equivalent to the particle diameter, because the dip-coated micelle encapsulated nanoclusters supported on oxidized substrates have been shown by TEM to be approximately spherical.[28]

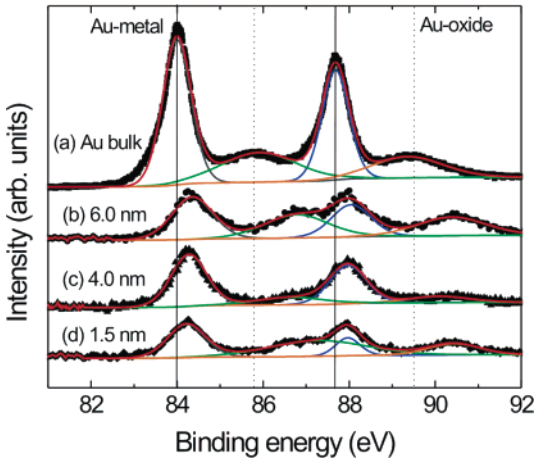

Figure 3. X-ray photoelectron spectra (Al Kα = 1486.6 eV) corresponding to the Au-4f core level of (a) a 100 nm thick electron-beam evaporated Au film deposited on Ti(100 nm)/Si(001), and Au nanoparticles with mean diameters of 6.0 nm (b), 4.0 nm (c), and 1.5 nm (d), supported on TiO_2/Ti-foil. All samples have been measured after O_2-plasma exposure (110 W, 300 mTorr, 10 min).

Electronic Properties: XPS. XPS measurements were performed after ex-situ removal of the polymer by the oxygen plasma. Figure 3b−d shows Au-4f core-level spectra for the Au-micelle samples deposited on a titanium foil as a function of average particle size (from 6.0 to 1.5 nm) after plasma exposure (within 1 h, sample transferred in air). A similarly treated 10 nm-thick continuous gold film electron-beam deposited on Ti(100 nm)/Si(001) (Figure 3a) was used as the bulk-Au reference for the binding energies of Au-metal and Au-oxide.

From the analysis of Figure 3, changes in the electronic properties of Au can be inferred from two observations associated with decreasing cluster size. First, a positive shift in the core binding energy of the Au^0 metal and Au^{3+} oxide peaks with respect to Au-bulk appears with decreasing cluster sizes. The binding energy of the Au^{3+} oxide peaks shifts more than those from Au^0; for example, shifts of +0.35 and +0.97 eV with respect to the 4f-Au peaks in Au^0 and Au_2O_3, respectively, were measured in 6 nm Au particles on TiO_2. The shift toward higher binding energies (Figure 3b−d) is also accompanied by a line broadening of the Au-4f spectrum relative to that of bulk Au (Figure 3a).

The magnitude and direction of these shifts are strongly dependent on the substrate,[29,30] as observed in Figure 4. These data show XPS spectra from Au nanoclusters on semiconducting titania (~15 nm) on Si(001), Ti-foil, insulating SiO_2 on Si(001), and conducting indium tin oxide (ITO) on glass. The resistance to oxidation as evidenced by the relative intensities and areas of the Au^0 to Au^{3+} peaks is size dependent on all supports, and each support type has a different binding energy shift.

Figure 4 shows XPS spectra for Au particles of average sizes of 6 nm (a), 4 nm (b), and 1.5 nm (c) supported on different oxide substrates and measured after exposure to the oxygen plasma. The subspectra fits to the raw data in Figure 4 reveal the presence of Au-metal and Au^{3+}-oxide, whose peaks shifted

(28) Palmer, R. E.; Pratontep, S.; Boyen, H. G. *Nature Materials* **2003**, *2*, 443.
(29) Radnik, R.; Mohr, C.; Claus, P. *Phys. Chem. Chem. Phys.* **2003**, *5*, 172−177.
(30) Dalacu, D.; Klemberg-Sapieha, J. E.; Martinu, L. *Surf. Sci.* **2001**, *472*, 33−40.

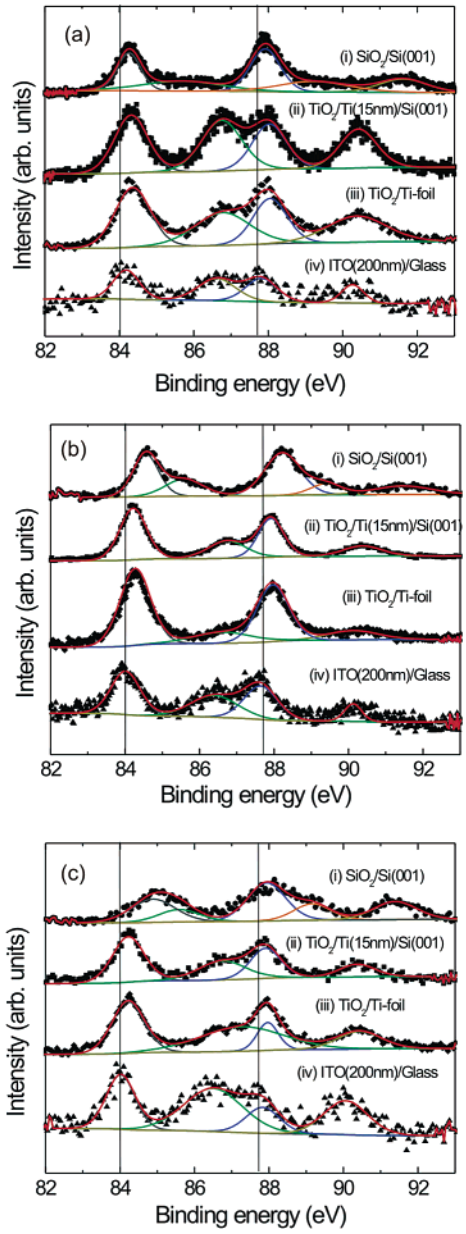

Figure 4. XPS spectra (Al Kα = 1486.6 eV) corresponding to the Au-4f core level of Au nanoclusters with average sizes of (a) 6.0 nm, (b) 4.0 nm, (c) 1.5 nm supported on SiO_2/Si(001), TiO_2/Ti(15 nm)/Si(001), TiO_2/Ti-foil, ITO(200 nm)/glass. All samples have been measured after O_2-plasma exposure (110 W, 300 mTorr, 10 min).

with respect to bulk gold as the size of the particles is reduced (Figure 5a).

Furthermore, for clusters with sizes of ~4 nm a lower Au^{3+} signal can be detected compared to the larger or smaller cluster sizes for all supporting substrates studied following identical oxygen plasma treatments. Although there will be a difference associated with the different surface-to-volume ratio, a relative resistance to reaction with the oxygen (metal-to-ligand charge transfer) is observed for the 4 nm clusters. This cluster size (as measured by AFM, and corresponding to 5 ± 1 nm as measured from TEM) is larger than the 1.4 nm Au_{55} clusters deposited on a native oxide silicon wafer that were found by Boyen et al.[21] to be resistant to oxidation.

We calculated the ratio of the peak areas from the fitted Au-oxide peaks to the fitted Au-metal peaks as a measure of the

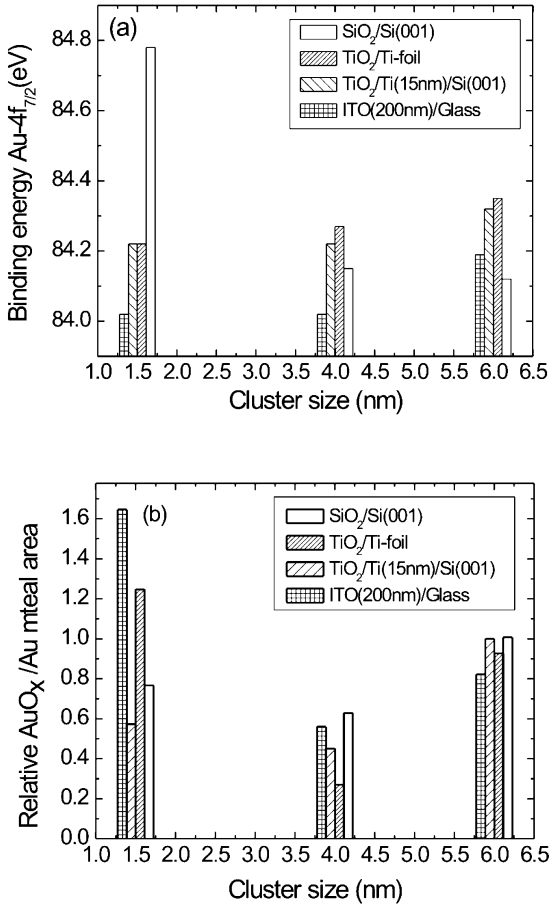

Figure 5. (a) XPS binding energies, and (b) relative AuO_x/Au spectral area obtained from a Gaussian−Lorentzian fit of Figure 4. The binding energies correspond to the Au-4f core level of Au nanoclusters supported on SiO_2/Si(001), TiO_2/Ti(15 nm)/Si(001), TiO_2/Ti-foil, and ITO(200 nm)/glass.

oxygen reactivity, Figure 5b, as a function of cluster size. The smallest Au clusters contained the largest fraction of surface oxide.

We also found that the Au-oxide layer formed after treating our Au-nanoclusters with oxygen plasma is stable over a longer period of time than what has been previously reported.[26] Tsai's group found that a Au_2O_3 overlayer formed on a continuous 100 nm thick Au film exhibited a half-life of 22 h for samples stored in air at 22 °C.[26] Our samples showed Au^{3+}-oxide as detected by XPS even after 6 weeks of sample exposure to ambient room conditions (not shown).

Figure 5a summarizes the binding energy shifts measured with respect to Au-bulk (Au-$4f_{7/2}$ = 84.0 eV) as a function of cluster size and support. An increase in the BE shift with decreasing cluster size has been observed for Au/SiO_2/n-Si(001) in accordance with Chusuei et al.[31] with a maximum shift of 0.88 eV at 1.5 nm.

The Au nanoparticles deposited on oxidized polycrystalline Ti substrates (Ti-foil) showed binding energy shifts similar to those of the TiO_2/Ti(15 nm) substrates with a maximum shift of 0.35 eV for 6 nm large particles. A slight decrease in BE was measured with decreasing particle size. The BE shifts obtained here are smaller than previous measurements reported

(31) Chusuei, C. C.; Lai, X.; Luo, K.; Goodman, D. W. *Top. Catal.* **2001**, *14*, 71−83.

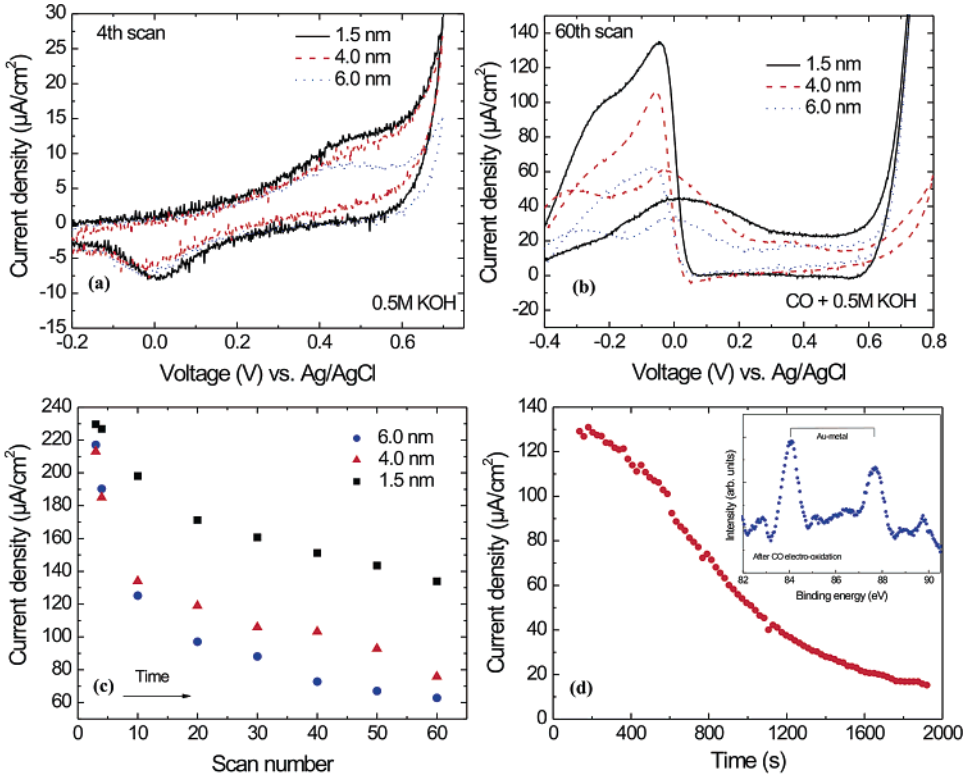

Figure 6. Cyclic voltammograms (IV) measured for three different average Au-cluster sizes: 1.5 nm (solid line), 4.0 nm (dashed line), 6.0 nm (dotted line) dip-coated onto ITO(200 nm)/glass substrates after saturation of a 0.5 M KOH solution with N_2 (fourth scan) (a), and with CO (60th scan) (b). (c) Current densities obtained at a fixed applied voltage (−0.07 V) versus IV scan number (increasing time) measured on 0.5 M KOH after CO saturation for Au clusters with sizes 1.5 nm (squares), 4.0 nm (triangles), 6.0 nm (circles). (d) Current density at a fixed voltage (−0.07 V) measured as a function of time for Au nanoparticles (4.0 nm) supported on ITO(200 nm)/glass in a 0.5 M KOH solution during continuous CO bubbling. The inset in (d) displays a XPS spectrum (Au-4f core level) of 4.0 nm Au nanoparticles measured after CO electrooxidation.

in the literature for thermally evaporated Au clusters supported on TiO_2 single crystals (up to 0.8 eV shift on TiO_2(110)).[31,32] It has been shown that the magnitude of the shift is strongly dependent on the oxide preparation conditions, specifically the defect concentration which will determine conductivity. Howard et al.[32] measured by XPS BE shifts 0.3 eV smaller on a defective TiO_2(110) surface as compared to a low-defect surface. On the polycrystalline TiO_2 surfaces, the defect density is higher than single-crystal TiO_2-rutile surfaces, hence the smaller observed BE shifts. The Au clusters supported on the conductive ITO substrate revealed a 0.17 eV decrease in BE when going from 6.0 to 1.5 nm cluster size, approaching the BE of bulk Au at 84.0 eV. An analogous decrease has been recently pointed out by Dalascu et al. [30]

Electrocatalytic Activity. The cyclic voltammograms measured for three different Au-cluster sizes on ITO/glass are shown in Figure 6. These scans were obtained after saturation of the 0.5 M KOH with N_2 (fourth scan, (a)), and after subsequent saturation with CO (60th scan, (b)). Current densities have been normalized to the effective gold surface area estimated by AFM and TEM images, assuming spherical Au nanoparticles. This normalization value is in good agreement with the Au-coverage that we can estimate from XPS measurements comparing the Au-metal peak strength (I_{Au-4f}) relative to the substrate peak strength (I_{Sn-5d}).

After N_2 saturation and prior to CO saturation, adsorption and desorption of oxygen was observed at +0.50 and 0.00 V versus Ag/AgCl, respectively, in agreement with previous literature reports,[25,33] Figure 6a. The presence of these peaks indicates that there is sufficient electrical contact between the ITO substrate and the Au clusters, and thus minimal electrical isolation was caused by residual polymer trapped under the clusters.

After CO saturation, Figure 6b, the Au oxidation and reduction peaks were no longer noticeable as compared to the stronger CO peaks. The primary CO oxidation peak was observed at −0.07 V while scanning in the cathodic direction. The smallest particles yielded the largest current densities for CO oxidation, approximately 135 μA/cm^2 after 60 IV scans, as compared to the medium and large particles that resulted in current densities of approximately 106 and 63 μA/cm^2, respectively. A thick bulk Au film prepared by PVD and measured under similar conditions showed no activity for CO oxidation.[25]

To further test the stability of the catalyst, successive cyclic voltammograms were measured after electrolyte saturation with CO, Figure 6c. With each consecutive cyclic voltammogram, the intensity of the CO oxidation peak decreased for all cluster sizes, although the small clusters were found to be active for a longer period of time. To elucidate the cause of the decrease in catalytic activity, a second set of cyclic voltammograms were measured for the medium size clusters (4 nm), this time with a constant CO concentration by continuous bubbling. Figure 6d displays the peak current densities extracted from IV scans measured at a fixed voltage of −0.07 V versus time. A decay

(32) Howard, A.; Clark, D. N. S.; Mitchell, C. E. J.; Egdell, R. G.; Dhanak, V. R. *Surf. Sci.* **2002**, *518*, 210−224.

(33) Maye, M.; Lou, Y. *Langmuir* **2000**, *16*, 7520.

in the activity was observed over time for these conditions as well, indicating that the decay was not a result of CO depletion. The presence of gold after CO electrooxidation has been confirmed by XPS (Figure 6d, inset).

Discussion

Electronic Properties: XPS. The Au-4f XPS spectra in Figures 3 and 4 were resolved into two doublets (spin−orbit splitting), one corresponding to pure gold and the other to nonmetallic gold (gold chloride or gold oxide). Previous literature reports[34,35] showed that Au_2O_3 is exclusively formed on the surface of Au^0 when exposed to an oxygen plasma. Additionally, no traces of chlorine were found by XPS on our samples after the oxygen plasma treatment.

The positive BE shifts shown in Figure 5a are contrary to what would be expected if one only considers the effect of an increase in the ratio of the number of incompletely coordinated surface atoms to the number of bulk atoms that occurs with decreasing cluster size. On polycrystalline gold,[3,36] for example, a 0.4 eV shift toward lower binding energies has been measured due to these "surface effects". There exist two mechanisms which can overcome the surface effect and produce a net positive BE shift in the core band: (1) initial- and (2) final-state effects.[37] The initial-state effects are related to the electronic structure of the clusters, and the final-state effects are a manifestation of the positive charge left on the surface of the cluster during the photoemission process. Which of the previously mentioned effects dominates in each particular metallic cluster−oxide support system is controversial.[3,38,39] Mason et al.[37] argued that changes in the cluster electronic structure are unavoidable as the particle size changes, and initial-state effects can never be neglected independently of the substrate used.[37] Final-state relaxation processes in the bulk will decrease the core binding energy (CBE) as compared to that of an isolated atom.[37,40] If the core-hole created during the photoemission process is not effectively screened, a positive BE shift will occur. The increase in the CBE with decreasing cluster size resulting from the disappearance of the bulk relaxation processes will be modulated by the substrate's ability to shield the final-state hole.

Competing with these processes is the possibility of cluster charging.[41] Core−electron photoemission from a positively charged cluster will have a higher CBE as a result of the Coulomb attraction barrier. This effect is dependent on the shape of the cluster[3] and image charge screening.[36] Whether or not charging is important depends on the ability of the substrate to neutralize the cluster within the lifetime of the core-hole. As an example, the BE shifts of up to ~0.22 eV for 1.7 nm large isolated Au nanocrystals (protected by PVP, and drop-casted on HOPG) measured by Thomas et al.[41] could be exclusively explained considering the charging of classical conducting particles.

Following Wertheim et al.,[3] the shifts to larger electron binding energies measured for small clusters supported on poorly conducting substrates have their origin in the positive charge of the cluster in the photoemission final state. We attribute the larger CBE shifts measured on Au particles deposited on SiO_2/Si(001) with decreasing size to a decreased contact area of the clusters with the substrate and a poorly conducting substrate that implies a less efficient charge neutralization to an excess positive charge distributed over the cluster's surface. The resulting Coulomb attraction will increase the apparent BE of the Au electrons by $\sim e^2/R$, where R is the cluster radius. Assuming spherical clusters (as demonstrated by cross-sectional high-resolution TEM images[28]), we can estimate the cluster radius as $\alpha e^2/\Delta BE$, where α is the Coulomb constant and ΔBE is the Au-4f energy shift. For the $Au/SiO_2/Si(001)$ system, the so calculated cluster diameters are 3.2, 5.4, and 11.0 nm. These values are 1.3−2 times larger than the sizes that we measured using transmission electron microscopy. The differences between calculated and measured values can be understood by taking into account relaxation terms from substrate contributions and surface effects that tend to decrease the shift, thus increasing the calculated radius.

The observed absence of a positive binding energy shift due to cluster charging in the Au/ITO system for the smaller clusters is a result of the ITO conductivity which allows for rapid neutralization of the clusters within the lifetime of the core-hole. The highly polarizable conduction electrons in the ITO will also mask any change in the final-state relaxation of the particles by providing efficient screening of the core-hole. The CBE shift and large line-widths for the ITO samples must be predominantly due to "initial-state" electronic structure effects.[30]

Together with the different binding energies observed for similar sized particles supported on substrates with different conductivities (Figure 5a), our work demonstrates that small Au nanoparticles can stabilize the otherwise thermodynamically unstable Au^{3+}-oxide phase (Figure 5b). Although the trends displayed in Figure 5b are valid qualitatively, we need to point out that the relative percentage of Au^{3+} estimated by XPS is higher than what would be measured using, for example, the extinction from surface plasmon resonances of gold nanoparticles,[42] because XPS will tend to overdetermine the fraction of Au^{3+} if it is more prevalent in the outermost volume of the particles.

The presence of a stable Au-oxide shell surrounding a metallic gold nanoparticle core is of crucial importance from the point of view of catalysis, because it may improve catalytic activity, as Over et al. demonstrated for the case of ruthenium and RuO_2.[43]

Electrocatalytic Activity. The high activity for CO oxidation displayed by the 1.5 nm nanoparticles as compared to the 4.0 and 6.0 nm particles (Figure 6b,c) may be a result of two factors: (1) size effects (resulting in a lower coordination number for surface atoms), and (2) stabilization of the Au^{3+}-oxide on the surface. If one would only consider the presence of Au-oxide as an exclusive parameter responsible for the enhanced catalytic activity observed, the medium-sized particles should be the least active according to our XPS data (Figure

(34) Maya, L.; Paranthaman, M.; Thundat, T.; Bauer, M. L. *J. Vac. Sci. Technol., B* **1996**, *14*, 15−21.
(35) Pireaux, J. J.; Liehr, M.; Thiry, P. A.; Delrue, J. P.; Caudano, R. *Surf. Sci.* **1984**, *141*, 221−232.
(36) Wertheim, G. K.; DiCenzo, S. B. *Phys. Rev. B* **1988**, *37*, 844.
(37) Mason, M. G. *Phys. Rev. B* **1983**, *27*, 748−762.
(38) DiCenzo, S. B.; Berry, S. D.; Hartford, E. H. *Phys. Rev. B* **1988**, *38*, 8465.
(39) Liang, K. S.; Salaneck, W. R.; Aksay, I. A. *Solid State Commun.* **1976**, *19*, 329.
(40) Lin, M. E.; Andres, R. P.; Reifenberger, R. *Phys. Rev. Lett.* **1991**, *67*, 477.
(41) Thomas, P. J.; Kulkami, G. U.; Rao, C. N. R. *Chem. Phys. Lett.* **2000**, *321*, 163−168.
(42) Swanson, N. L.; Billard, B. D. *Nanotechnology* **2003**, *14*, 353−357.
(43) Over, H.; Kim, Y. D.; Seitsonen, A. P.; Wendt, S.; Lundgren, E.; Schmid, M.; Varga, P.; Morgante, A.; Ertl, G. *Science* **2000**, *287*, 1474−1476.

5b), in contradiction with the electrochemical reactivity observations. Our results give evidence for an overall significant size-dependency in the electrocatalytic activity of Au nanoparticles synthesized by diblock copolymer encapsulation.

The catalyst deactivation observed (Figure 6c) may be due to several processes including: (1) carbon poisoning on the catalyst surface passivating the active sites, (2) Au surface contamination by deposition of K from the electrolyte (0.5 M KOH solution), and (3) etching of Au resulting in fewer sites.

XPS studies performed after CO electrocatalysis showed that the deactivation observed is fundamentally due to potassium. A strong K-2p peak was observed by XPS after electrooxidation, indicating that K is deposited on the sample surface during the IV measurement. K is known to promote the adsorption and stabilization of CO_2 on metal surfaces, thus eliminating the catalytically active surface sites.[44] A loss of 30−40% of the Au was also observed after 60 cyclic voltammograms (3).

Conclusions

The interdependence of cluster size and cluster−support interactions in the unique electronic and chemical properties displayed by oxide-supported noble metal nanoparticles has been demonstrated. Size- and support-dependent binding energy shifts were found, and an increased (positive) binding energy was observed with decreasing cluster size and decreasing support conductivity. A nonmonotonic dependence of oxygen reactivity on cluster size and support was found. The stabilization of surface Au^{3+}-oxide on the small Au clusters especially reactive with oxygen has been shown to correlate with the increase in the activity for CO electrooxidation.

Acknowledgment. The research is partially supported by the U.S. Department of Energy (DE-FG03-89ER14048) and the U.S. Air Force Office of Scientific Research (DURINT grant F49620-01-1-0459). This work made use of the MRL Central Facilities supported by the National Science Foundation under award DMR96-32716 and the UCSB Nanofabrication Facility. We would also like to thank Dr. Tom Mates, Ms. Anna Ivanovskaya, and Mr. Michael Sushchikh for technical assistance and helpful discussions.

JA036468U

(44) Freund, H. J.; Roberts, M. W. *Surf. Sci. Rep.* **1996**, *25*, 225−273.